Demonstration of Inverse Acoustic Band Gap Structures in AlN and Integration with Piezoelectric Contour Mode Wideband Transducers

Nai-Kuei Kuo, Chengjie Zuo, and Gianluca Piazza
Department of Electrical and Systems Engineering
University of Pennsylvania, Pennsylvania
Philadelphia, USA
kuo1@seas.upenn.edu

***Abstract*—This paper presents the first design and demonstration of a novel inverse acoustic band gap (IABG) structure in aluminum nitride (AlN) and its direct integration with contour-mode wideband transducers in the Very High Frequency (VHF) range. This design implements an efficient approach to co-fabricate in-plane AlN electro-acoustic transducers with bulk acoustic waves (BAWs) IABG arrays (10x10). The IABG unit cell consists of a cylindrical high acoustic velocity (*V*) media, which is held by four thin tethers, surrounded by a low acoustic velocity matrix (air). The center media is formed by 2-μm-thick AlN, which is sandwiched by 200-nm-thick top and bottom platinum (Pt) layers. The experimental results indicate that the designed IABG has a stop band from 185 MHz to 240 MHz and is centered at 218 MHz in the Γ-X direction. This demonstration not only confirms the existence of the frequency band gap in the IABG structure, but also opens possibilities for the integration of ABG structures with RF MEMS devices.**

I. INTRODUCTION

In recent years, research activities in acoustic wave applications have focused on the design of phononic crystals (PCs) because of their potential advantages in the making of more efficient, and compact ultrasonic devices [1]. However, there have been only very few bulk acoustic wave (BAW) demonstrations in the Very High Frequency (VHF) range [2, 3]. These acoustic band gap (ABG) structures are based on a conventional cell arrangement formed by a high acoustic velocity (*V*) matrix with low acoustic velocity inclusions. As in photonic crystals, the mismatch between the material properties of the unit cell and the periodic arrangement of the cells prohibit the propagation of acoustic waves within certain frequencies: this is known as the frequency band gap. The operating frequency range is determined by the lattice constant, *a*, and it is inversely proportional to it. For bulk ABG structures, the behavior of the stop band is highly dependent on the material mismatch [4] and the dimensional parameters (the radius of inclusion, *r*, and the thickness, *d*) [5]. The focus of the research on micro-scale ABGs has been to maximize the width of the band gap by altering the shape or material composition of the unit cell. In Mohammadi's work [2], the frequency stop band was effectively increased by introducing a hexagonal lattice structure. As a result, the separation between the two fundamental Bragg resonant frequencies increased, and correspondingly enlarged the complete frequency band gap [4]. However, this design requires the thickness of the structural layer to be nearly the same of the lattice constant. This poses some challenges in the making of thick ABG structures and prevents the direct integration of the ABGs within the same plane of the electro-acoustic devices used to provide the interface between the electrical and acoustic domains.

This work presents the design of a novel inverse acoustic band gap (IABG) structure whose unit cell is formed by center cylindrical high acoustic velocity material (aluminum nitride, AlN, and platinum, Pt) held by four thin tethers and surrounded by low acoustic velocity material (air). The simulations from COMSOL® Finite Element Method (FEM) multi-physics software indicate that this cell arrangement induces a wider frequency band gap than the conventional ABG structure with similar dimensional parameters. Moreover, the IABG structure can maintain a band gap even with thin films (*d/a* = 0.23) and additional metal layer depositions (Pt). This solution offers the advantage of direct integration of the IABG with Very High Frequency (VHF) piezoelectric contour-mode (CM) transducers, which require AlN film thicknesses of 1-2 μm [6]. Furthermore, the ability to include metals in the IABG material stack offers the possibility of directly integrating the IABG as supporting elements for RF MEMS devices. More importantly, the FEM analysis suggests that the center and width of the frequency stop band induced by this new ABG structure not only depend on the *r/a* and *d/a* ratios, but also on a unique feature of this design, the tether width. This characteristics enables additional freedom in setting the frequency band gap.

978-1-4244-3510-4/09/$25.00 ©2009 IEEE

II. DESIGN OF THE INVERSE ACOUSTIC BAND GAP STRUCTURE AND THE WIDEBAND TRANSDUCERS

A. *The Inverse Acoustic Band gap (IABG) Structure*

The unit cell of the IABG structure is presented in Fig. 1. The principal dimensions of the cell are the lattice constant, *a*, the radius, *r*, the thickness, *d*, and the tether width, *w*.

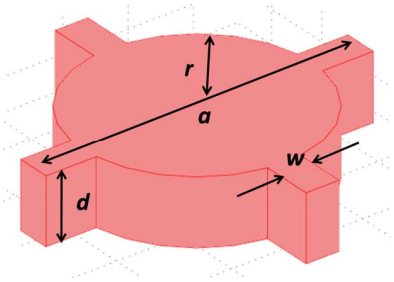

Figure 1. Unit cell and key parameters of the IABG structure

In order to directly integrate the IABG array in the same plane of the contour-mode wideband devices, the thickness of the IABG structure is set to be the same of the electro-acoustic transducers, which are formed, in the VHF range, by 2-µm-thick AlN and 200-nm-thick top and bottom Pt layers. The predicted frequency band gap is simulated by COMOSL® Finite Element Method (FEM) Multi-physics software. This approach has been discussed in previous work by Gorishnyy [7]. The acoustic wave traveling inside a periodic media is described by the elastic wave equation and Bloch-Floquet theorem [8]. In the FEM simulation, the eigenfrequencies of the ABG array are found by solving the elastic wave equation with periodic boundary conditions applied to the unit cell. However, these eigenfrequencies only represent the vibration modes for a certain wavevector. The complete dispersion relationship is obtained by finding all the eigenfrequencies for the main symmetric directions of the first Brillouin zone (Γ-X-M-Γ) of the reciprocal lattice [9]. The normalized frequency band gap (frequency multiplied by *a*) response of the AlN IABG is presented in Fig. 2, for which the thickness of AlN and Pt are fixed at 2 µm and 200 nm, respectively.

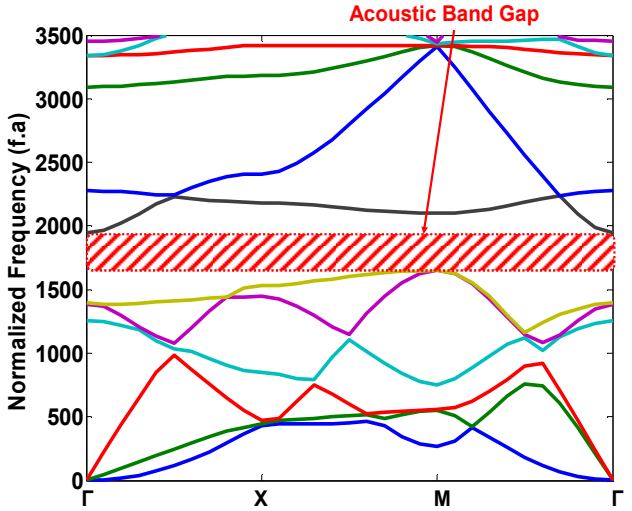

Figure 2. The dispersion relationship of the IABG structure simulated in COMSOL®

The behavior of the stop band in the VHF range was further analyzed in COMSOL® to characterize its response with respect to the radius, *r*, and the tether width, *w*. By keeping the lattice and tether width constant (a = 8 µm, w = 1 µm), the radius, *r*, was varied between 2 and 3.5 µm and the frequency response of the IABG was analyzed (Fig. 3). Differently from the conventional ABG structures [2], the band gap properties show a nonlinear dependence on the *r/a* ratio. As shown in Fig. 3, the maximum bandwidth occurs when the radius is equal to 2.9 µm (*r/a* ~ 0.37). In order to have a frequency band gap with gap-to-midgap ratio greater than 15 %, the *r/a* ratio should be defined to be between 0.36 and 0.375. More importantly, the results indicate that changes in radius have a greater effect on the gap-to-midgap ratio (maximum change of ~ 5 % per 100 nm change in radius) than the center of the band gap (maximum change of ~ 2 % per 100 nm change in radius).

Despite the high sensitivity of the gap-to-midgap ratio to the radius, the bandwidth of the bandgap can also be controlled by the tether width, *w*, therefore relaxing the requirements on the *r/a* ratio. The simulated results in fact indicate that the bandwidth of the frequency stop band is also significantly impacted by the tether width. Fig. 3 also indicates that the frequency band gap changes with the tether width. There is an approximately linear relationship between the band gap and the size of tether width. The center frequency of the stop band decreases with the tether width (~ 2 % per 100 nm change in the tether width); however, the size of the band gap increases as the width decreases (~ 5-6 % per 100 nm change in the tether width).

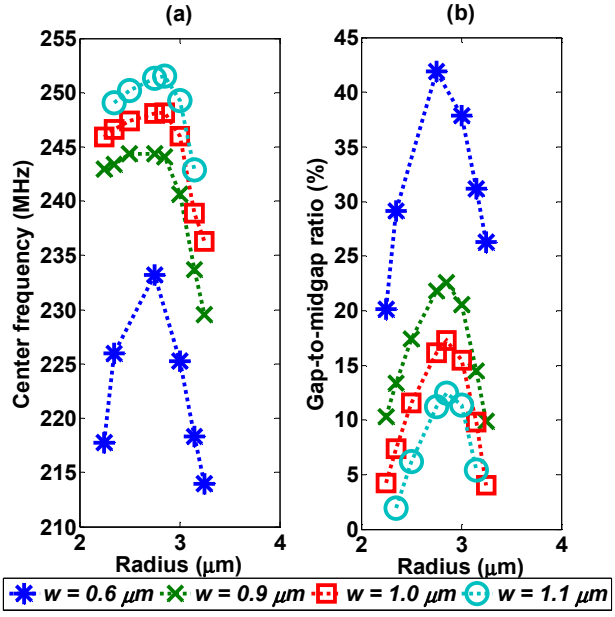

Figure 3. The frequency band gap response of the IABG as a function of radius for a constant lattice (a = 8 µm) dimension and various tether width dimensions. (a) Center frequency and (b) the gap-to-midgap ratio are plotted with respect to the radius, *r*. The analysis was performed in COMSOL®

For the purpose of this demonstration, the lattice constant was set to be 8.6 µm for operation at 218 MHz. This frequency was selected because reliable operation of piezoelectric contour-mode device in this frequency range had

been previously demonstrated [10]. In order to obtain a sufficiently wide bulk acoustic band gap, the size of the radius was designed to be 3.3 µm (r/a ~ 0.38). On the other hand, due to limitation in the fabrication process, the tether width was set to be 1 µm.

B. *AlN Piezoelectric Contour-Mode Wideband Transducers*

The AlN piezoelectric contour-mode (CM) wideband transducers consist of two contour-mode resonators (CMRs) [6] with slanted fingers. These electro-acoustic transducers induce lateral bulk vibrations via the piezoelectric properties of the AlN thin film, The transducers launch directly bulk acoustic waves (BAWs) into the coupled IABG array. The operating frequency of a device with constant width, W, is given by:

$$f_o = \frac{1}{2W}\sqrt{\frac{E_{eq}}{\rho_{eq}}} \tag{1}$$

On the other hand, the slanted finger technique is based on varying the width of the transducers along the length of the device and enables the generation of a wider frequency response. This technique was previously demonstrated for surface acoustic waves (SAWs) [11]. The maximum (W_{low}) and minimum (W_{high}) widths of the slanted finger determine the bandwidth (Δf) of the transducer, which can be approximately calculated analytically:

$$\Delta f \propto \frac{1}{W_{high}} - \frac{1}{W_{low}} \tag{2}$$

This method to generate a wideband response is implemented with the AlN CM transducers so that an effective in-plane BAW over a wide frequency range can propagate inside the IABG structure.

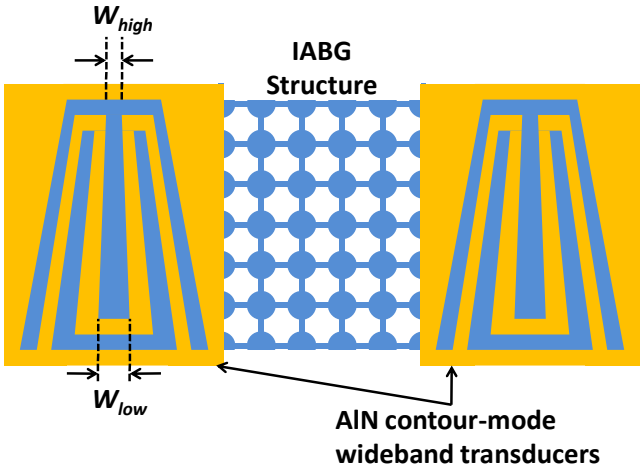

Figure 4. Mock-up representation of the piezoelectric wideband transducers with the IABG structure

The slanted finger was chosen to have a width varying between 17 and 25 µm, which induces a range of bulk acoustic waves with frequencies from 175 MHz to 257 MHz.

III. Experimental Results and Discussion

The IABG structure integrated with the AlN CM wideband transducers was fabricated in a four-mask and post-CMOS compatible micro-fabrication process similar to the one reported in [12]. Another set of the wideband transducers coupled by a plate was also fabricated with the same process and employed as a reference to experimentally verify the existence of the acoustic band gap. The transmission response of the IABG structure was measured via an Agilent N5230 PNA-L Network Analyzer after performing a standard short-open-load-through (SOLT) calibration. The extracted data from the IABG structure were further impedance-matched to eliminate electrical losses and focus exclusively on the acoustic characteristic of the device.

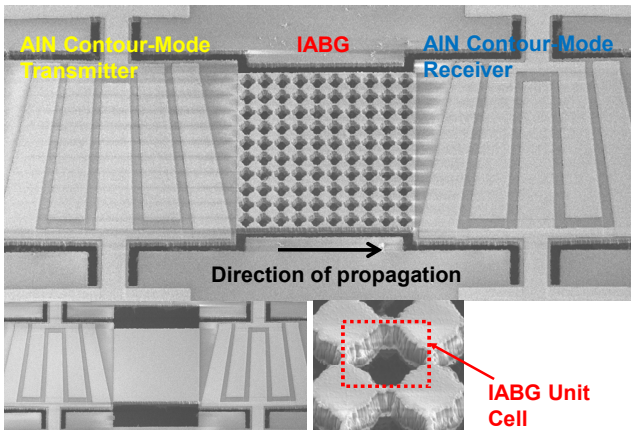

Figure 5. Scanning Electron Microscope (SEM) image of the micro-fabricated IABG structure coupled by the wideband transducers. Inset on the left is the reference transducers and slab. Inset on the right is the IABG unit cell.

The experimental results verified the existence of the frequency band gap, as shown in Fig. 6. The complete acoustic band gap occurs between 185 MHz and 240 MHz, and is centered at 218 MHz.

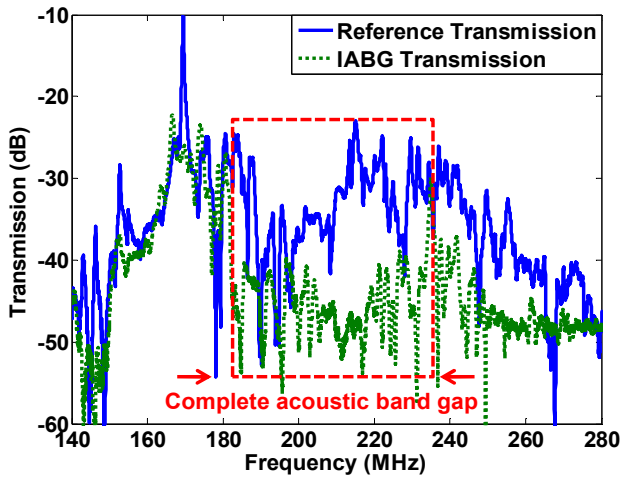

Figure 6. The experimental transmission responses from the IABG and the reference structures

Although a wide frequency range of bulk acoustic waves was induced by the transducers, the reference response indicates that there is a reduced transmission between 190 and

200 MHz. This does not permit to establish in full the effectiveness of the IABG in this frequency range. In addition, the measured complete band gap appears to have a larger bandwidth than the simulated response. In particular the IABG shows additional rejection at higher frequencies (250 to 280 MHz). This is likely due to the fact that the CM devices primarily induce bulk acoustic waves propagating in the [100] direction (Γ-X).

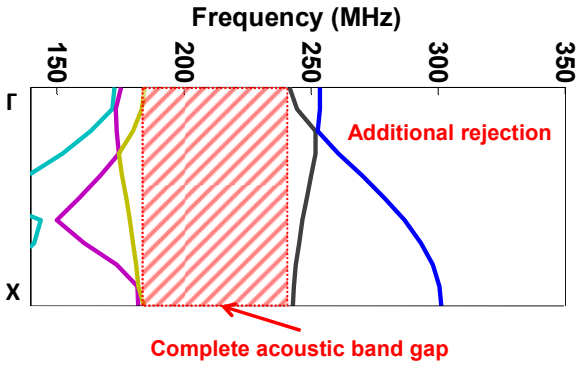

Figure 7. Zoomed in view of the dispersion curve generated via COMSOL simulations and showing that a wider band gap exists in the Γ-X direction

In fact the stop band in the Γ-X direction as simulated in COMSOL (Fig.7) is wider than the complete bang gap and is consistent with the experimental response. Thus, this demonstration has successfully presented the existence of the complete frequency band gap induced by the IABG structure. The designed frequency band gap (Γ-X) centers at 218 MHz with rejection between 185 MHz and 240 MHz.

IV. Conclusion

In this work, the frequency stop band induced by the inverse acoustic band gap (IABG) structure in aluminum nitride (AlN) has been analyzed and experimentally demonstrated. The dependence of the IABG center frequency and bandwidth on the key dimensional parameters has also been studied and shows that even wider band gap can be set by acting on the *r/a* ratio or the tether width. The existence of a wide frequency stop band for small *d/a* ratio not only relaxes the restrictions on the film thickness, but also permits the direct integration with electro-acoustic transducers. At the same time, the inclusion of metal layers in the IABG structure enables electrical routing on the IABG for their integration with RF MEMS devices. For instance, the IABG structure can be adopted to replace the anchors of existing piezoelectric contour-mode resonators (CMRs). The current bar-shaped anchor is in fact one of the main sources of energy losses in the resonator. By replacing the anchor with the IABG structure, acoustic wave propagation through it will be forbidden, and therefore the quality factor, *Q*, of the device will be enhanced.

This first very high frequency (VHF) demonstration of the IABG opens the pathway for the development of PC-based devices for RF communication. Similarly to photonic crystals, the IABG structure can be used to realize devices such as waveguides and filters. Future research will focus on improving the fabrication process of the IABG to scale its operation to the ultra high frequency (> 1 GHz) range.

Acknowledgment

The authors would like to offer special thanks to the Wolf Nanofabrication Facility staff at Penn for their assistance with part of the fabrication process and the Tegal Corporation for the AlN deposition. Also, we greatly appreciate the help from Dr. Watson and Dr. Gaevski with the platinum deposition at the PRISM Micro/Nanofabrication Lab in Princeton.

References

[1] Y. Pennec, B. Djafari-J. O. Vasseur, and H. Larabi, "Acoustic channel drop tunneling in a phononic crystal," Appl. Phys. Lett., vol. 87, 261912, Decemebr 2005

[2] S, Mohammadi, A. A. Eftekhar, A. Khelif, W. D. Hunt, and A. Adibi, "Evidence of large high frequency complete phononic band gaps in silicon phononic crystal plates," Appl. Phys. Lett., vol. 92, 221905, June 2008

[3] R. Olsson III, J. Fleming, I. El-Kady, M. Tunk, and F. McCormick, "Micromachined bulk wave acoustic band gap devices," Tech. Digest, International Conf. on Solid-State Sensors, Actuators, and Microsystems, Lyon, France, June 2007, pp. 317-321

[4] R Olsson III and I El-Kady, "Microfabricated phononic crystal devices and applications," Meas. Sci. Technol., vol. 20, 012002, November 2008

[5] S. Mohammadi, A. A. Eftekhar, A. Khelif, H. Moubchir, R. Westafer, W. D. Hunt, and A. Adibi, "Complete phononic bandgaps and bandgap maps in two-dimensional silicon phononic crystal plates," Elec. Lett., vol. 43, No. 16, August 2007

[6] C. Zuo, N. Sinha, C. R. Perez, R. Mahameed, M. B. Pisani, G. Piazza, "Hybrid ultra-compact 4th order band-pass filter based on piezoelectric AlN contour-mode MEMS resonators," Solid-State Sensors, and Microsystems, Hilton Head Island, SC, USA, June 2008, pp. 324-327

[7] T. Gorishnyy, C. K. Ullal, M. Maldovan, G. Fytas, E. L. Thomas, "Hypersonic Phononic Crystals," Phys. Rev. Lett., vol. 94, issue 11, 115501, 2005

[8] P. Langlet, A.-C. Hladky-Hennion, and J.-N. Decarpigny, "Analysis of the propagation of plane acoustic waves in passive periodic materials using the finite element method," J. Acoust. Soc. Am., vol. 98, issue 5, pp. 2792-2800, November 1995

[9] C. Kittel, "Introduction to Solid State Physics," John Wiley & Sons, Inc., New Jersey, 2005

[10] C. Zuo, N. Sinha, J. Van der Spiegel, and G. Piazza, "Multi-frequency pierce ocsillators based on piezoelectric AlN contour-mode MEMs resontros," 2008 IEEE International Frequency Control Symposium, May 2008, pp. 402-407

[11] M. Goto, H. Yatsuda, T. Chiba, "Optimum design for slanted finger SAW filters on langasite substrate," IEEE Ultrasonics Symposium, Vancouver, Canada, October, 2006, pp. 192-195

[12] N. Sinha, R. Mahameed, C. Zuo, M. B. Pisani, C. R. Perez, and G. Piazza, "Dual-beam actuation of piezoelectric AlN RF switches monlithically integrated with contout-mode resonators," Solid-State Sensors, and Microsystems, Hilton Head Island, SC, USA, June 2008, pp. 22-25